Journal of Biomechanics 129 (2021) 110815

Contents lists available at ScienceDirect

Journal of Biomechanics

journal homepage: www.elsevier.com/locate/jbiomech

Depth-dependent patterns in shear modulus of temporomandibular joint cartilage correspond to tissue structure and anatomic location

Cassandra J. Gologorsky [a], Jill M. Middendorf [b], Itai Cohen [c], Lawrence J. Bonassar [a,b,*]

[a] Meinig School of Biomedical Engineering, Cornell University, Ithaca, NY, USA
[b] Sibley School of Mechanical and Aerospace Engineering, Cornell University, Ithaca, NY, USA
[c] Department of Physics, Cornell University, Clark Hall C7, Ithaca, NY 14853, USA

ARTICLE INFO

Keywords:
Digital image correlation
Elastography
TMJ disorders
Cartilage
Fibrocartilage

ABSTRACT

To fully understand TMJ cartilage degeneration and appropriate repair mechanisms, it is critical to understand the native structure-mechanics relationships of TMJ cartilage and any local variation that may occur in the tissue. Here, we used confocal elastography and digital image correlation to measure the depth-dependent shear properties as well as the structural properties of TMJ cartilage at different anatomic locations on the condyle to identify depth-dependent changes in shear mechanics and structure. We found that samples at every anatomic location showed qualitatively similar shear modulus profiles as a function of depth. In every sample, four distinct zones of mechanical behavior were observed, with shear modulus values spanning 3–5 orders of magnitude across zones. However, quantitative characteristics of shear modulus profiles varied by anatomic location, particularly zone size and location, with the most significant variation in zonal width occurring in the fibrocartilage surface layer (zone 1). This anatomic variation suggests that different locations on the TMJ condyle may play unique mechanical roles in TMJ function. Furthermore, zones identified in the mechanical data corresponded on a sample-by-sample basis to zones identified in the structural data, indicating the known structural zones of TMJ cartilage may also play unique mechanical roles in TMJ function.

1. Introduction

The temporomandibular joint (TMJ) connects the jaw to the skull and is frequently the site of temporomandibular joint disorders (TMJDs). These disorders affect over 10 million people annually in the United States (Wadhwa and Kapila, 2008). TMJDs are characterized by biomechanical malfunctions such as clicking, locking, and joint misalignment (Singh and Detamore, 2009) andmanifest as jaw pain and limited range of motion (Wadhwa and Kapila, 2008). These symptoms are present during talking, chewing, and any action involving jaw motion (Singh and Detamore, 2009), leading to a decreased quality of life (Kuroda et al., 2009; Wadhwa and Kapila, 2008). Because the mechanism of TMJD is unknown and its onset cannot be predicted, there is no standard therapeutic approach for treatment (Sharma et al., 2011; Wadhwa and Kapila, 2008).

TMJDs involve mechanical damage and failure of TMJ cartilage (Kuroda et al., 2009; Wadhwa and Kapila, 2008). Despite its primarily mechanical role, little is known about the mechanical properties of TMJ cartilage or their relationship to TMJ cartilage structure. In particular, the shear mechanics of TMJ cartilage have not been studied extensively, despite the prevalence of shearing in the TMJ resulting from grinding motions during chewing (Kuroda et al., 2009; Singh and Detamore, 2009; Teramoto et al., 2003). As such, it is critical to understand the global and local structure-mechanics relationships of TMJ cartilage.

Structurally, TMJ cartilage is composed of four distinct zones (Singh and Detamore, 2009; Wadhwa and Kapila, 2008). Unlike hyaline cartilage from other joints, TMJ cartilage has a surface layer composed of highly aligned type I collagen fibers (Kuroda et al., 2009). This fibrocartilage surface layer cushions the joint from peak loads by dissipating shear forces during jaw motion (Kuroda et al., 2009; Wadhwa and Kapila, 2008), reducing cartilage deformation during compression, and reducing friction (Ruggiero et al., 2015). Below the fibrocartilage layer, there are three additional zones: proliferative, mature, and hypertrophic, which are similar to three zones in hyaline cartilage (Wadhwa and Kapila, 2008). Notably, the mechanical properties of each zone remain largely unknown, particularly the shear properties.

* Corresponding author at: Daljit S. and Elaine Sarkaria Professor, Meinig School of Biomedical Engineering, Sibley School of Mechanical and Aerospace Engineering, 149 Weill Hall, Cornell University, Ithaca, NY 14853, USA.
E-mail address: lb244@cornell.edu (L.J. Bonassar).

https://doi.org/10.1016/j.jbiomech.2021.110815
Accepted 8 October 2021
Available online 15 October 2021

Global shear modulus of TMJ cartilage has previously been shown to vary with direction (i.e. anisotropy), frequency, and load magnitude (Tanaka et al., 2008). Lateral regions of the TMJ were found to be thicker (Burrows and Smith, 2007) with a higher compressive modulus than other anatomic regions (Singh and Detamore, 2009), while posterior regions had a lower modulus (Tanaka et al., 2006). However, local shear mechanics of the TMJ have not yet been studied, and this remains a significant gap in our understanding of TMJ cartilage function, degeneration, and repair.

Recent studies have documented methods to measure local properties of other types of cartilage (Buckley et al., 2010, 2008) and have connected the depth-dependent zonal structure of hyaline cartilage to its mechanical function (Griffin et al., 2015; Henak et al., 2016; Middendorf et al., 2017; Silverberg et al., 2014), Silverberg et al., 2013). However, this technique has never been applied to study depth-dependent TMJ cartilage shear mechanics.

To address this gap in knowledge, we analyzed the depth-dependent shear properties of TMJ cartilage at different anatomic locations on the condyle to identify local changes in shear mechanics. We also analyzed depth-dependent TMJ cartilage structure at different anatomic locations via histology. The length scales of these structural and mechanical features were then compared across five anatomic locations to determine how the relationships between these features change with position on the joint.

2. Materials and methods

2.1. Sample preparation

TMJ condyles were extracted from five 6–7-month-old porcine heads of mixed sex sourced from a local butchery (Schrader Farms Meat Market, Romulus, NY). A total of 35 osteochondral cores (5 mm diameter) from five different anatomic locations on each condyle (anterior, posterior, medial, lateral, central) were bisected to produce paired hemicylindrical samples (Fig. 1A) used for mechanical testing and histological staining. This approach enabled a direct comparison between mechanical properties and structural organization for each sample.

2.2. Mechanical testing

Prior to shear testing, the subchondral bone side and the sliced rectangular side of each hemicylindrical sample were cryotomed to ensure flat, perpendicular surfaces for mounting and visualization. As described previously (Buckley et al., 2010), samples were stained in 14 μg/mL 5-dichlorotriazinyl-aminofluorescein (5-DTAF) (Sigma, St. Louis, MO) for visualization (Fig. 1B, i) under an inverted Zeiss LSM 510 5 live confocal microscope (Carl Zeiss AG, Oberkochen, Germany) to image the rectangular cross-section of each hemicylinder (Fig. 1B, ii). The cartilage was compressed to 10% global axial strain and allowed to equilibrate for twenty minutes, and five lines were photobleached onto samples in order to track tissue deformation (Fig. 1B, iv). A 1% oscillatory shear strain was applied to the sample at a rate of 1 Hz (Fig. 1B, iii) to mimic the rate of human jaw motion during chewing, and videos were recorded (Fig. 1B, iv-v)

2.2.1. Data analysis

To extract shear modulus from videos, a MATLAB (Mathworks, Natick, MA) algorithm was used to track photobleached lines (Buckley et al., 2013). Lines were tracked over 20 cycles of shear strain and used to develop a plot of maximum marker displacement amplitude as a function of cartilage depth, and strains were calculated by taking the derivative of the displacement with respect to depth. Applied forces were calculated from calibrated springs attached to the stationary plate, and these forces were divided by sample area to calculate shear stress. Shear stress was divided by shear strain as a function of depth to obtain a plot of shear modulus as a function of depth. Mechanically distinct zones in each sample were determined by identifying the maximum slope of the shear modulus versus depth curve.

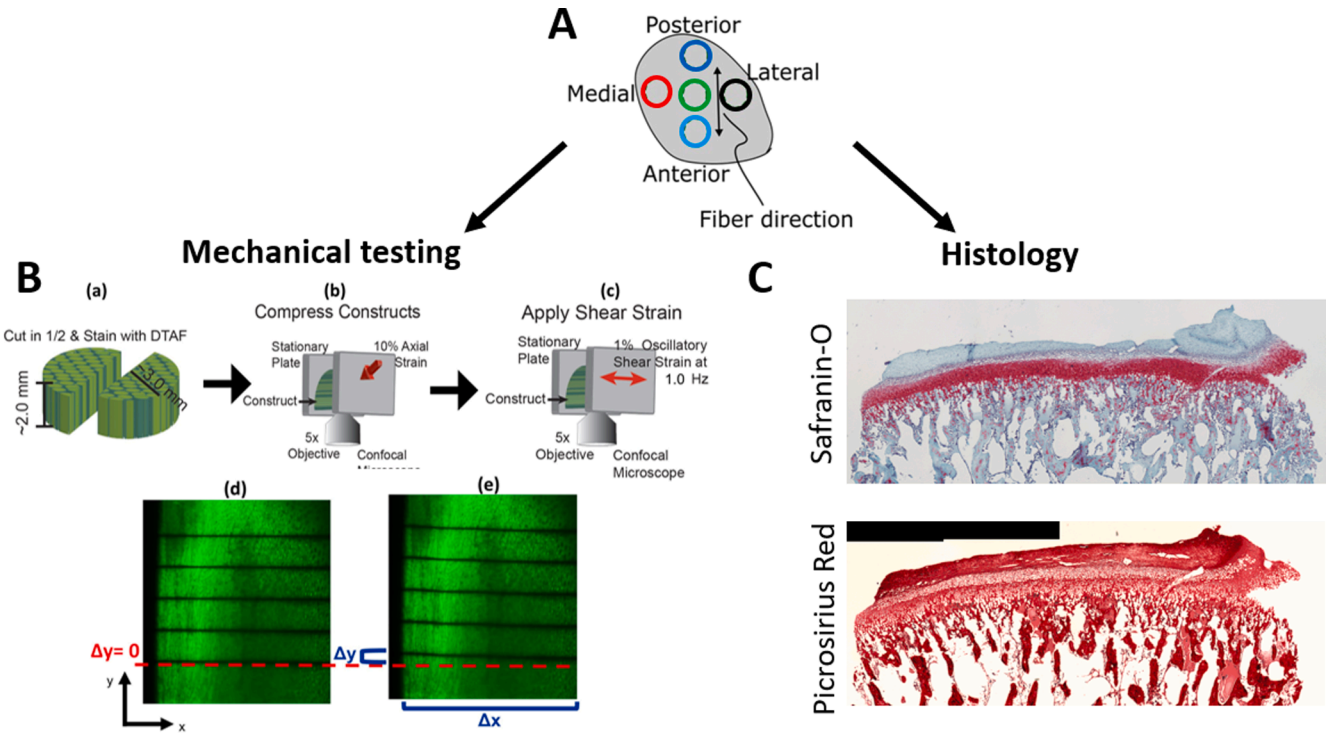

Fig. 1. Overview of experimental setup for mechanical and structural analysis of TMJ condylar cartilage. Hemicylindrical samples were extracted from five anatomic locations on the TMJ condyle (A) and bisected in the anteroposterior (AP) direction. One hemicylinder from each pair underwent mechanical testing (B) while the other was sectioned and stained to analyze structural elements (C).

2.2.2. Statistical analysis

Variation of shear modulus magnitude in samples was compared across all zones using an analysis of variance (ANOVA) with repeated measures, with pairwise comparisons performed via multiple t-tests with Bonferroni correction. Variation of zonal thickness, total sample thickness, and zonal modulus magnitude across anatomic locations were compared using a one-way ANOVA with a Tukey post-hoc test. All statistical analyses were performed using R-studio (R Foundation for Statistical Computing, Vienna, Austria).

2.2.3. Histology

Samples for histology were prepared by the Clinical Pathology Core at the Cornell College of Veterinary Medicine. Briefly, samples were fixed in neutral buffered formalin (Fisher Scientific, Pittsburg, PA) for 48 h, rinsed with ethanol, decalcified, and embedded in paraffin. Several 4 μm sections were obtained and stained with Safranin-O to observe relative proteoglycan content or Picrosirius red to observe relative collagen content (Fig. 1C). Sections were then imaged under a light microscope (Nikon Eclipse TE2000-S, Microvideo Instruments, Avon, MA) and analyzed in ImageJ (Rueden et al., 2017). Structural features, including collagen staining, proteoglycan staining, and cellular content, were used to identify and measure TMJ cartilage zone thicknesses.

3. Results

Samples from different anatomic locations showed qualitatively

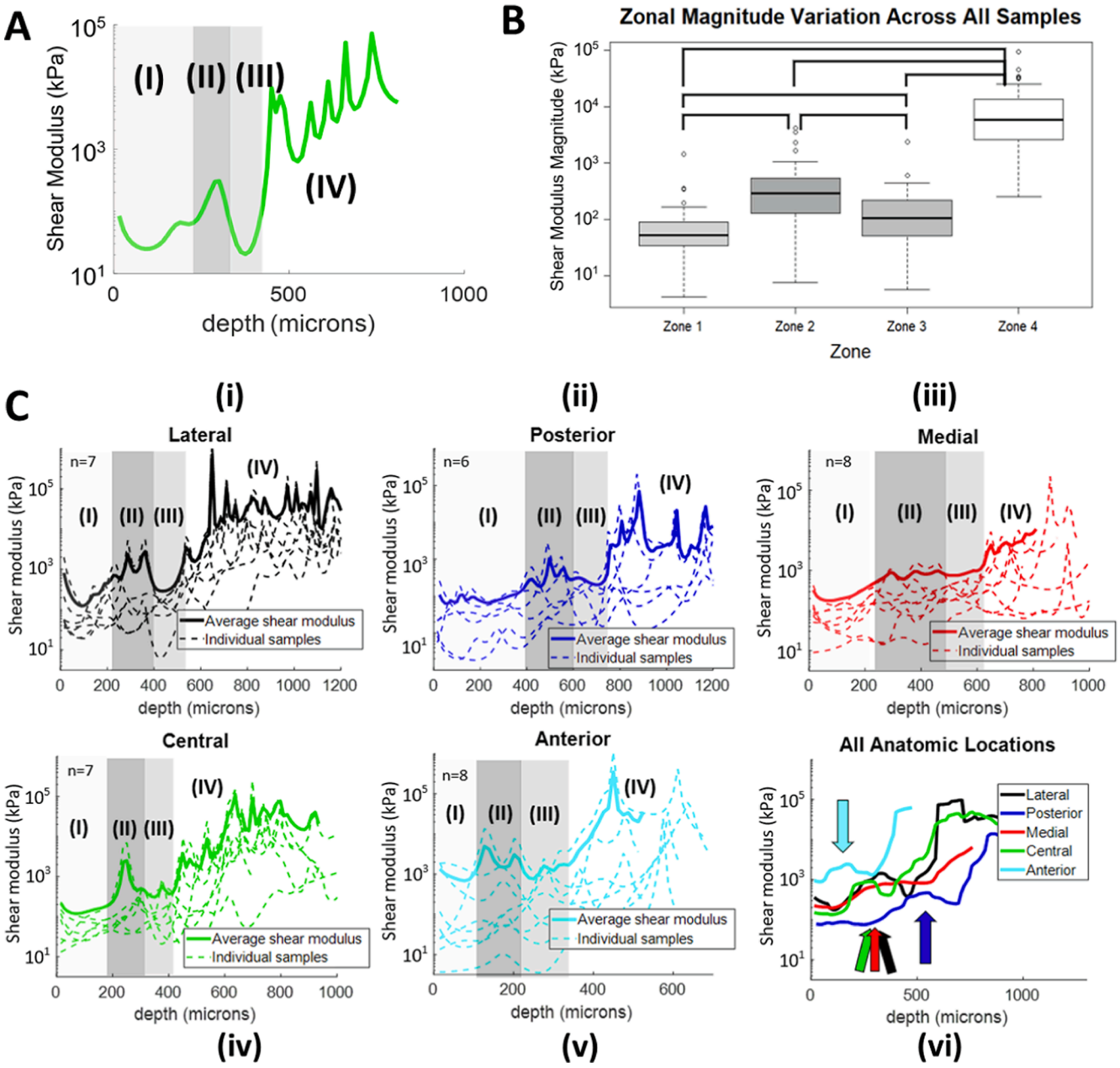

Fig. 2. Analysis of shear modulus as a function of depth and anatomic location. (A) Example shear modulus profile showing qualitative shear modulus variation over depth. In one sample, the shear modulus spans over 4–5 orders of magnitude. (B) Summary table showing modulus changes observed across zones in all samples, with bars representing statistically significant comparisons. All zones are statistically different from one another ($p < 0.05$ for all comparisons). (C) Shear modulus profiles from lateral (i), posterior (ii), medial (iii), central (iv), and anterior (v) regions. Individual samples are plotted as dotted lines, with the cohort average plotted as a solid, thicker line. The cohort averages of all regions were plotted together to more clearly identify variation among anatomic locations (vi). Arrows indicate the difference in depth at which the average local maximum in zone II occurs for each anatomic location.

similar depth-dependent shear modulus profiles. Each sample had four distinct zones of mechanical behavior, with a local shear modulus maximum in the second zone and a global maximum in the fourth zone. (Fig. 2A). Shear modulus was lowest in zone 1 (95% CI: 1.15×10^2 kPa $\pm$ 8.32×10^1 kPa), increased slightly in zone 2 (95% CI: 6.03×10^2 kPa $\pm$ 3.25×10^2 kPa), and decreased slightly in zone 3 (95% CI: 2.1×10^2 kPa $\pm$ 1.37×10^2 kPa) before increasing to its maximum values in zone 4 (95% CI: 1.24×10^4 kPa $\pm$ 6.193×10^3 kPa) (Fig. 2B). The shear modulus magnitude of each zone did not vary across anatomic locations (p values ranging from 0.466 to 0.999, Supplementary Fig. S1), suggesting that shear properties of each zone do not vary with anatomic location.

While samples had qualitatively similar shear modulus profiles, quantitative characteristics of profiles varied by anatomic location. In particular, the width and position of each zone varied with anatomic location (Fig. 3A), most prominently in zone 1. Posterior samples were 2–3 times thicker in zone 1 than all other regions (post-ant, $p = 8 \times 10^{-7}$; post-cent, $p = 2.3 \times 10^{-4}$; post-lat, $p = 6.5 \times 10^{-5}$; post-med, $p = 2.7 \times 10^{-4}$) (Fig. 3Ai). Anterior samples were nominally 20–30% thinner in zone 1 than medial, central, and lateral regions (med-ant, $p = 0.26$; lat-ant, $p = 0.56$; cent-ant, $p = 0.29$). Zones 2 and 4 varied slightly, with medial samples having the thickest average zone 2 ($p = 0.015$) and anterior samples having the thinnest zone 4 ($p = 7.29 \times 10^{-3}$) (Fig. 3A, ii and iv). Although zone 3 did not vary in width by location, the variations observed in zones 1 and 2 indicated that zone 3 occurred at different tissue depths for different anatomic locations. The overall cartilage thickness at each anatomic location also varied, with lateral, medial, and posterior samples having thicker cartilage than anterior and central regions (Fig. 3B).

Safranin-O and Picrosirius red staining revealed four distinct structural zones (Fig. 4A, C). Zone 1 had a high collagen content and no proteoglycans, while zone 2 had a slightly lower collagen content and an increase in nuclear staining, indicating greater cell density. Zone 3 had relatively lower collagen content than zone 2 but showed an increase in proteoglycan content, while zone 4 showed the least collagen content, the highest proteoglycan content, and the appearance of hypertrophic chondrocytes. These four observed structural regions are consistent with the four structural zones of TMJ cartilage identified in literature (Kuroda et al., 2009; Singh and Detamore, 2009; Wadhwa and Kapila, 2008).

After observing four distinct zones of mechanical behavior in shear modulus profiles and four structural zones in histology data, mechanical and structural data were compared on a sample-by-sample basis. At each location, structural data from each sample was compared to mechanical data from the corresponding hemicylinder (Fig. 4B, C). By aligning histological and mechanical data, we identified a strong visual correspondence between the identified structural zones and mechanical zones from multiple anatomic locations (Fig. 4B, C, Supplementary Fig. S2).

In all samples, the first mechanical zone of low modulus corresponded to the first structural zone of high collagen and low proteoglycan content, while the second mechanical zone of a local modulus maximum corresponded to the second structural zone of decreased collagen and increased cell density. The third mechanical zone of decreased shear modulus corresponded to the third structural zone with a slight increase in proteoglycan content and a slight decrease in collagen content, and the fourth mechanical zone of an absolute shear modulus maximum corresponded to the fourth structural zone characterized by dense proteoglycans and the appearance of hypertrophic chondrocytes.

The relationship between zonal widths from mechanical and histological analyses were compared in a correlation plot (Fig. 4D). Zonal width was calculated from the mechanical data using an algorithm to find inflection points of a curve fitted to the data; the inflection points

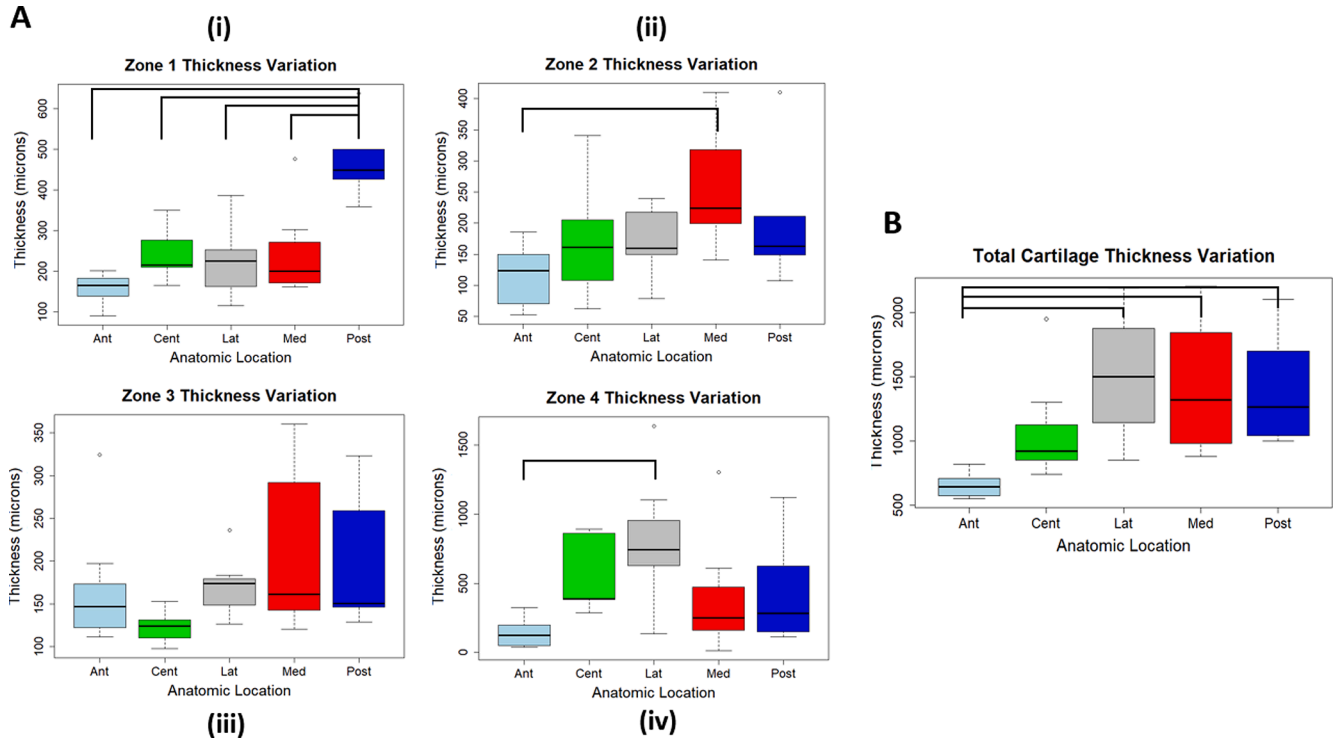

Fig. 3. Zonal thickness and overall cartilage thickness by anatomic location. Bars represent statistically significant comparisons. (A)(i) Zone 1 thickness ranged from 90 to 640 μm among all samples; posterior samples had a significantly larger zone 1 than all other anatomic locations (post-ant, $p = 8 \times 10^{-7}$; post-cent, $p = 2.276 \times 10^{-4}$; post-lat, $p = 2.276 \times 10^{-4}$; post-med, $p = 2.276 \times 10^{-4}$). (ii) Zone 2 thickness ranged from 50 to 410 μm, with a significant different between anterior and medial regions ($p = 0.015$). (iii). Zone 3 thickness ranged from 100 to 360 μm and did not vary significantly among anatomic locations (Supplemental Fig. S1)(iv) Zone 4 thickness ranged from 60 to 1640 μm, with a significant difference between anterior and lateral regions ($p = 7.29 \times 10–3$). (B). Overall cartilage thickness ranged from 550 to 2200 μm, with anterior samples having the smallest average thickness of all anatomic locations (ant-lat, $p = 4.08 \times 10^{-3}$; ant-med, $p = 4.08 \times 10^{-3}$; ant-post, $p = 2.26 \times 10^{-2}$).

A

Zone	Relative proteoglycan content	Relative collagen content	Other features
I	None	High	
II	None/Low	High/Medium	Increased cellularity
III	Medium/High	Medium/Low	
IV	High	Low	Appearance of chondrocytes

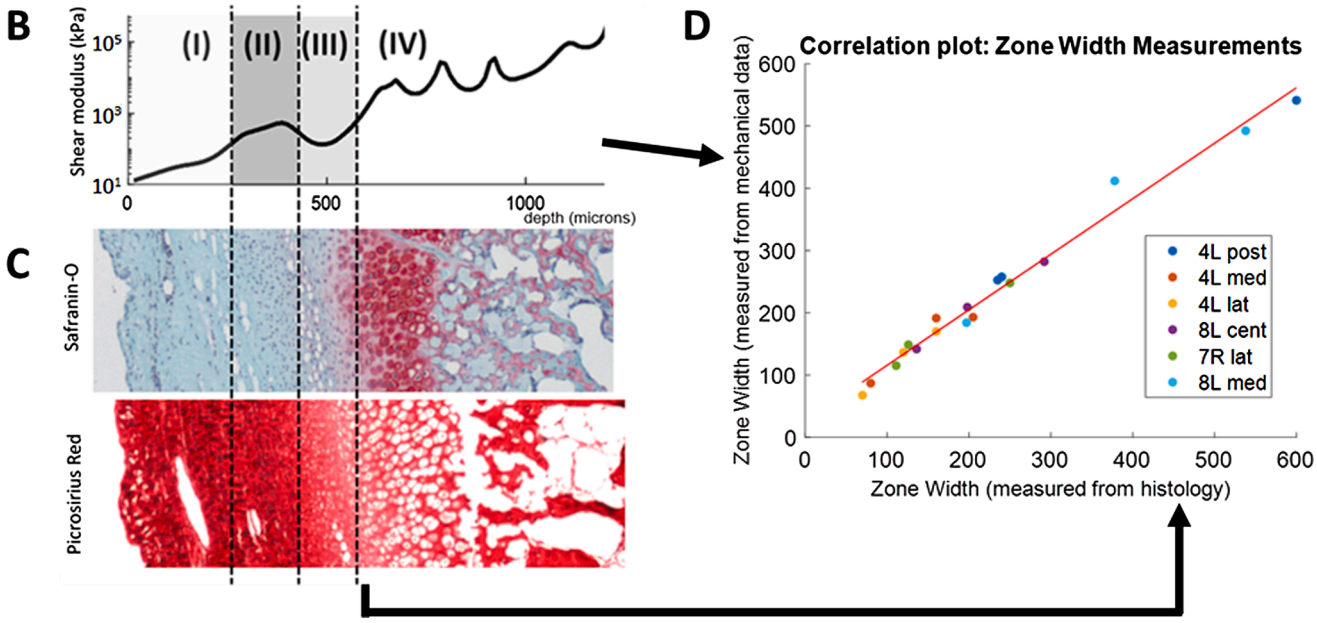

Fig. 4. Histology analysis and correlation between mechanical and structural zones. Four structural zones of TMJ cartilage (A) were identified from structural features observed in histology (C). A visual correlation was observed between structural and mechanical zones on a sample-by-sample basis (B, C), and this visual correlation was quantified with a correlation plot (D).

represent the approximate start and end points of each zone. Zonal width from histology was calculated by measuring visually distinct regions in ImageJ based on zonal characteristics specified earlier. The resulting plot showed high correlation between zone lengths measured from mechanical data and histology data ($R^2 = 0.981$, $p = 2.74 \times 10^{-15}$). Notably, the slope of the correlation plot was around 0.89 rather than 1, consistent with 10% compression imposed during mechanical testing, while histological samples were fixed in an uncompressed state.

4. Discussion

This study identified a correlation between TMJ cartilage mechanics and TMJ cartilage structure, showing four distinct mechanical zones that correspond to four distinct structural zones. These mechanically distinct zones behave in radically different ways and vary in shear modulus by multiple orders of magnitude, suggesting that known structural zones of TMJ cartilage have unique mechanical roles. In addition to mechanical variation observed between zones, the thickness and location of each zone also varied with anatomic location on the condyle, suggesting that different anatomic locations also perform unique mechanical roles. Collectively, these data demonstrate that TMJ condylar cartilage has important depth-dependent structural and mechanical features that are not observed in hyaline cartilage from other joints.

The zonal changes in shear modulus are consistent with the observed changes in collagen and proteoglycan content in TMJ cartilage. The second and fourth zones, which were the stiffest, had intense staining for collagen (zone 2) or proteoglycans (zone 4). In contrast, the first and third zones were the most compliant. Overall, relative zonal increases in collagen or proteoglycans correlated well with localized increases in the shear modulus of TMJ cartilage.

Notably, the collagen in zone 1 is highly aligned in the direction of shearing (Singh and Detamore, 2009; Tanaka et al., 2008), which would enable a high degree of inter-fiber sliding. This is consistent with the known role of zone 1 in dispelling frictional forces caused by jaw movement (Wadhwa and Kapila, 2008). It is also known that zone 2 serves as a cell reservoir for proliferating cells, while zone 3 provides resistance against compressive and lateral forces (Wadhwa and Kapila, 2008). This information is consistent with the fact that Zone 3 had the least intense staining for both collagen and proteoglycans, suggesting that this region had the lowest matrix density and a relatively low shear modulus. In articular cartilage, matrix density has been shown to have a profound effect on shear modulus (Silverberg et al., 2014). Therefore, the drop in shear modulus between zone 2 and zone 3 is likely due to the aforementioned difference in matrix density between these two zones. Furthermore, this drop in modulus in zone 3 means there are higher levels of strain present during loading in zone 3. Higher levels of strain are known to cause mitochondrial damage, which suggests that zone 3 cells may be more susceptible to damage during injurious loading (Ayala et al., 2021; Bartell et al., 2015; Bonnevie et al., 2018).

Despite these correlations, the quantitative relationships between structure, composition, and mechanics in TMJ cartilage remain unknown. A main challenge in identifying quantitative relationships between structure and mechanics is the qualitative nature of histology. Previous work has examined quantitative relationships between tissue composition, structure, and mechanics of both hyaline cartilage and fibrocartilage using advanced microscopy tools such as FTIR microspectroscopy (DiDomenico et al., 2019; Middendorf et al., 2020; Silverberg et al., 2014), Raman spectroscopy (Boys et al., 2019), and multiphoton microscopy (DiDomenico et al., 2019). Additionally, mechanistic frameworks such as rigidity-percolation simulations have been applied to model the relationship between composition, structure, and mechanical properties of hyaline cartilage (Silverberg et al., 2014). These quantitative approaches could shed additional light on how the zonal structure of TMJ cartilage gives rise to local shear mechanics.

This study also demonstrated important variations in mechanical properties based on anatomic location. This variation is consistent with previous studies demonstrating that the lateral region has the highest compressive modulus (Singh and Detamore, 2009). We found that the lateral region had a relatively thin zone 1 and zone 3 (the weakest zones) and a thick zone 4 (the strongest region). Similarly, reports of a low indentation modulus in the posterior region (Tanaka et al., 2006) are consistent with our observation that the posterior region has a thick surface zone that is highly compliant. Similarly, the anatomic variation in overall cartilage thickness observed here is consistent with previous studies in primates and further supports the idea that each anatomic location plays a different mechanical role (Burrows and Smith, 2007).

The majority of anatomic variation in zonal width was found in the fibrous surface zone (zone 1). This variability in the surface zone is consistent with previous studies of articular cartilage from the knee (Silverberg et al., 2013) and ankle (Henak et al., 2016), which demonstrated that anatomic variations in hyaline cartilage were greatest in the surface region. Further, previous studies of TMJ cartilage mechanics noted that the structural anisotropy in the fibrous zone of porcine TMJ cartilage is believed to contribute to shear mechanical anisotropy (Singh and Detamore, 2009) and anatomic differences in friction (Middendorf et al., 2019). The extent to which these variations in zonal structure by anatomic location are driven by local variations in mechanical loading and susceptibility to disease is currently unknown.

Notably, zonal shear modulus magnitude did not vary across anatomic locations, suggesting that global anatomic variations are driven by the ratios of zonal thickness at each site. However, the statistical similarity observed across anatomic locations may be a result of large variations in overall shear modulus observed on an animal-by-animal basis (i.e. type II error). Since eight joints were used from five different animals, this resulted in a wide range of average shear moduli for each zone, even within one anatomic location (Zone 1: 4.2–1.43 $\times$ 10^3 kPa; Zone 2: 7.64–4.21 $\times$ 10^3 kPa; Zone 3: 5.7–2.39 $\times$ 10^3 kPa; Zone 4: 2.54 $\times$ 10^2–9.26 $\times$ 10^4 kPa).

The importance of structure in dictating local mechanics is further highlighted by mechanical abnormalities in some samples that corresponded to structure abnormalities (Supplementary Fig. S3). Notably, fingerlike protrusions of collagen-rich, proteoglycan-free tissue were found protruding into zone 4 (Supplementary Fig. S3A), and these regions were found to have abnormally low shear modulus. Both the mechanics and structure of these protrusions were similar to zone 1, indicating a possible role for fibrous collagen in lowering tissue modulus. In another sample, only one distinct mechanical zone was observed (Supplementary Fig. S3B), which also only showed similarity to zone 1 and lacked zones 2–4. Analysis of such samples highlights the effectiveness of elastography in identifying minor mechanical abnormalities.

Understanding depth-dependent variation in TMJ cartilage is essential for further understanding of tissue failure in TMJD and for identifying adequate treatment options to restore the TMJ. Many efforts have been made to re-engineer the TMJ (Aryaei et al., 2016; Wang and Detamore, 2007), but these methods do not consider zonal or anatomic variations. Similarly, establishing mechanical and zonal variation allows for the development of accurate TMJ models to better understand potential disease mechanisms or treatments (Liu et al., 2016; Sagl et al., 2019). All zones should be considered when assessing TMJ degeneration and repair, and the structural and architectural components of each layer may be needed to recapitulate the native healthy function of the TMJ for appropriate tissue- and joint-scale models.

It should be noted that these studies were performed on young porcine tissue of mixed sex. It was assumed that there would be minimal degradation of tissue based on the young age of the animals, but a more formal grading of the histology images would be needed to confirm this. Additionally, although quantitative differences in male and female TMJ shear modulus were not addressed in this study, it would be valuable to consider sex in future studies due to clinical differences in TMJ disease between men and women. Similarly, both the age and difference in species of the porcine samples may also affect quantitative measurements of total thickness, zonal thickness, and shear modulus. However, many studies have previously established the use of porcine samples to model the human TMJ (Herring, 2003; Tanaka et al., 2006), because porcine TMJ recapitulates the multiplanar motion and three-dimensional shape of the TMJ condyle in adult humans (Herring, 2003). With this in mind, our approach and results also provide valuable data for better understanding porcine models in future TMJ studies.

Furthermore, all data in this study was collected at one frequency and amplitude. A frequency of 1 Hz was chosen to mimic the rate of human jaw motion during chewing, but this does not encompass the full range of frequencies the mandibular joint experiences. Previous work has demonstrated that the local shear properties of hyaline cartilage have a clear frequency dependence (Buckley et al., 2013) and amplitude dependence (Buckley et al., 2008). Similarly, global TMJ shear properties vary with shearing frequency and amplitude (Tanaka et al., 2008). As such, future studies should consider the frequency-dependence and amplitude-dependence of local TMJ cartilage shear properties.

Lastly, there are technical challenges in measuring moduli across multiple orders of magnitude. The increased stiffness of zone 4 resulted in very small displacements (0.05–0.5 μm), which is near the limit of resolution for our technique. This limitation has also been noted in previous work using confocal elastography to map microscale shear properties of articular cartilage (Buckley et al., 2010) using b-spline fitting or data smoothing algorithms.

This study used state of the art tools in micromechanical testing to identify key zonal and anatomic variations in cartilage from the TMJ condyle. Shear moduli varied by more than 3 orders of magnitude through the depth of the tissue, with zonal variations in mechanics correlating highly with zonal variations in structure. These data give new and important insight into anatomic variations in the depth-dependent function of healthy TMJ cartilage.

Declaration of Competing Interest

The authors declare that they have no known competing financial interests or personal relationships that could have appeared to influence the work reported in this paper.

Acknowledgements

The authors would like to thank Jingyang Zheng, Thomas Wyse Jackson, and Eric Yoon for their technical expertise and training on confocal elastography.

This research was partially funded by NSF CMMI 1927197 and an NSF Graduate Research Fellowship (JM).

CG, JM, IC, and LB were involved in the planning of studies, interpretation of data, as well as writing and editing the manuscript. CG and JM were responsible for executing all experiments.

Appendix A. Supplementary material

Supplementary data to this article can be found online at https://doi.org/10.1016/j.jbiomech.2021.110815.

References

Aryaei, A., Vapniarsky, N., Hu, J.C., Athanasiou, K.A., 2016. Recent tissue engineering advances for the treatment of temporomandibular joint disorders. Curr. Osteoporos. Rep. 14, 269–279. https://doi.org/10.1007/s11914-016-0327-y.

Ayala, S., Delco, M.L., Fortier, L.A., Cohen, I., Bonassar, L.J., 2021. Cartilage articulation exacerbates chondrocyte damage and death after impact injury. J. Orthop. Res. Off. Publ. Orthop. Res. Soc. 39, 2130–2140. https://doi.org/10.1002/jor.24936.

Bartell, L.R., Fortier, L.A., Bonassar, L.J., Cohen, I., 2015. Measuring microscale strain fields in articular cartilage during rapid impact reveals thresholds for chondrocyte death and a protective role for the superficial layer. J. Biomech. 48, 3440–3446. https://doi.org/10.1016/j.jbiomech.2015.05.035.

Bonnevie, E.D., Delco, M.L., Bartell, L.R., Jasty, N., Cohen, I., Fortier, L.A., Bonassar, L.J., 2018. Microscale frictional strains determine chondrocyte fate in loaded cartilage. J. Biomech. 74, 72–78. https://doi.org/10.1016/j.jbiomech.2018.04.020.

Boys, A.J., Kunitake, J.A.M.R., Henak, C.R., Cohen, I., Estroff, L.A., Bonassar, L.J., 2019. Understanding the stiff-to-compliant transition of the meniscal attachments by spatial correlation of composition, structure, and mechanics. ACS Appl. Mater. Interfaces 11, 26559–26570. https://doi.org/10.1021/acsami.9b03595.

Buckley, M.R., Bergou, A.J., Fouchard, J., Bonassar, L.J., Cohen, I., 2010. High-resolution spatial mapping of shear properties in cartilage. J. Biomech. 43, 796–800. https://doi.org/10.1016/j.jbiomech.2009.10.012.

Buckley, M.R., Bonassar, L.J., Cohen, I., 2013. Localization of viscous behavior and shear energy dissipation in articular cartilage under dynamic shear loading. J. Biomech. Eng. 135 https://doi.org/10.1115/1.4007454.

Buckley, M.R., Gleghorn, J.P., Bonassar, L.J., Cohen, I., 2008. Mapping the depth dependence of shear properties in articular cartilage. J. Biomech. 41, 2430–2437. https://doi.org/10.1016/j.jbiomech.2008.05.021.

Burrows, A.M., Smith, T.D., 2007. Histomorphology of the mandibular condylar cartilage in greater galagos (Otolemur spp.). Am. J. Primatol. 69, 36–45. https://doi.org/10.1002/ajp.20325.

DiDomenico, C.D., Kaghazchi, A., Bonassar, L.J., 2019. Measurement of local diffusion and composition in degraded articular cartilage reveals the unique role of surface structure in controlling macromolecular transport. J. Biomech. 82, 38–45. https://doi.org/10.1016/j.jbiomech.2018.10.019.

Griffin, D.J., Bonnevie, E.D., Lachowsky, D.J., Hart, J.C.A., Sparks, H.D., Moran, N., Matthews, G., Nixon, A.J., Cohen, I., Bonassar, L.J., 2015. Mechanical characterization of matrix-induced autologous chondrocyte implantation (MACI®) grafts in an equine model at 53 weeks. J. Biomech. 48, 1944–1949. https://doi.org/10.1016/j.jbiomech.2015.04.010.

Henak, C.R., Ross, K.A., Bonnevie, E.D., Fortier, L.A., Cohen, I., Kennedy, J.G., Bonassar, L.J., 2016. Human talar and femoral cartilage have distinct mechanical properties near the articular surface. J. Biomech. 49, 3320–3327. https://doi.org/10.1016/j.jbiomech.2016.08.016.

Herring, S.W., 2003. TMJ anatomy and animal models. J. Musculoskelet. Neuronal Interact. 3, 391–394.

Kuroda, S., Tanimoto, K., Izawa, T., Fujihara, S., Koolstra, J.H., Tanaka, E., 2009. Biomechanical and biochemical characteristics of the mandibular condylar cartilage. Osteoarthr. Cartil. 17, 1408–1415. https://doi.org/10.1016/j.joca.2009.04.025.

Liu, Z., Qian, Y., Zhang, Y., Fan, Y., 2016. Effects of several temporomandibular disorders on the stress distributions of temporomandibular joint: a finite element analysis. Comput. Methods Biomech. Biomed. Eng. 19, 137–143. https://doi.org/10.1080/10255842.2014.996876.

Middendorf, J., Albahrani, S., Bonassar, L.J., 2019. Stribeck Curve Analysis of Temporomandibular Joint Condylar Cartilage and Disc. J. Biomech. Eng. https://doi.org/10.1115/1.4045283.

Middendorf, J.M., Dugopolski, C., Kennedy, S., Blahut, E., Cohen, I., Bonassar, L.J., 2020. Heterogeneous matrix deposition in human tissue engineered cartilage changes the local shear modulus and resistance to local construct buckling. J. Biomech. 105, 109760 https://doi.org/10.1016/j.jbiomech.2020.109760.

Middendorf, J.M., Griffin, D.J., Shortkroff, S., Dugopolski, C., Kennedy, S., Siemiatkoski, J., Cohen, I., Bonassar, L.J., 2017. Mechanical properties and structure-function relationships of human chondrocyte-seeded cartilage constructs after in vitro culture. J. Orthop. Res. 35, 2298–2306. https://doi.org/10.1002/jor.23535.

Rueden, C.T., Schindelin, J., Hiner, M.C., DeZonia, B.E., Walter, A.E., Arena, E.T., Eliceiri, K.W., 2017. Image J2: ImageJ for the next generation of scientific image data. BMC Bioinf. 18, 1–26. https://doi.org/10.1186/s12859-017-1934-z.

Ruggiero, L., Zimmerman, B.K., Park, M., Han, L., Wang, L., Burris, D.L., Lu, X.L., 2015. Roles of the fibrous superficial zone in the mechanical behavior of TMJ condylar cartilage. Ann. Biomed. Eng. 43, 2652–2662. https://doi.org/10.1007/s10439-015-1320-9.

Sagl, B., Schmid-Schwap, M., Piehslinger, E., Kundi, M., Stavness, I., 2019. A dynamic jaw model with a finite-element temporomandibular joint. Front. Physiol. 10, 1–12. https://doi.org/10.3389/fphys.2019.01156.

Sharma, S., Gupta, D.S., Pal, U.S., Jurel, S.K., 2011. Etiological factors of temporomandibular joint disorders. Natl. J. Maxillofac. Surg. 2, 116–119. https://doi.org/10.4103/0975-5950.94463.

Silverberg, J.L., Barrett, A.R., Das, M., Petersen, P.B., Bonassar, L.J., Cohen, I., 2014. Structure-function relations and rigidity percolation in the shear properties of articular cartilage. Biophys. J. 107, 1721–1730. https://doi.org/10.1016/j.bpj.2014.08.011.

Silverberg, J.L., Dillavou, S., Bonassar, L., Cohen, I., 2013. Anatomic variation of depth-dependent mechanical properties in neonatal bovine articular cartilage. J. Orthop. Res. 31, 686–691. https://doi.org/10.1002/jor.22303.

Singh, M., Detamore, M.S., 2009. Biomechanical properties of the mandibular condylar cartilage and their relevance to the TMJ disc. J. Biomech. 42, 405–417. https://doi.org/10.1016/j.jbiomech.2008.12.012.

Tanaka, E., Iwabuchi, Y., Rego, E.B., Koolstra, J.H., Yamano, E., Hasegawa, T., Kawazoe, A., Kawai, N., Tanne, K., 2008. Dynamic shear behavior of mandibular condylar cartilage is dependent on testing direction. J. Biomech. 41, 1119–1123. https://doi.org/10.1016/j.jbiomech.2007.12.012.

Tanaka, E., Yamano, E., Dalla-Bona, D.A., Watanabe, M., Inubushi, T., Shirakura, M., Sano, R., Takahashi, K., van Eijden, T., Tanne, K., 2006. Dynamic compressive properties of the mandibular condylar cartilage. J. Dent. Res. 85, 571–575. https://doi.org/10.1177/154405910608500618.

Teramoto, M., Kaneko, S., Shibata, S., Yanagishita, M., Soma, K., 2003. Effect of compressive forces on extracellular matrix in rat mandibular condylar cartilage. J. Bone Miner. Metab. 21, 276–286. https://doi.org/10.1007/s00774-003-0421-y.

Wadhwa, S., Kapila, S., 2008. TMJ disorders: future innovations in diagnostics and therapeutics. J. Dent. Educ. 72, 930–947.

Wang, L., Detamore, M.S., 2007. Tissue engineering the mandibular condyle. Tissue Eng. 13, 1955–1971. https://doi.org/10.1089/ten.2006.0152.